

Combined inclusive diffractive cross sections measured with forward proton spectrometers in deep inelastic ep scattering at HERA

The H1 and ZEUS Collaborations

F.D. Aaron^{14,e}, H. Abramowicz^{72,as}, I. Abt⁵⁷, L. Adamczyk³⁶, M. Adamus⁸⁵, R. Aggarwal^{15,m}, C. Alexa¹⁴, V. Andreev⁵⁴, S. Antonelli¹¹, P. Antonioli¹⁰, A. Antonov⁵⁵, M. Arneodo⁷⁸, O. Arslan¹², V. Aushev^{39,40,ak}, Y. Aushev^{40,ak,al}, O. Bachynska³⁰, S. Backovic⁶⁵, A. Baghdasaryan⁸⁷, S. Baghdasaryan⁸⁷, A. Bamberger²⁶, A.N. Barakbaev², G. Barbagli²⁴, G. Bari¹⁰, F. Barreiro⁵⁰, E. Barrelet⁶⁴, W. Bartel³⁰, N. Bartosik³⁰, D. Bartsch¹², M. Basile¹¹, K. Begzsuren⁸¹, O. Behnke³⁰, J. Behr³⁰, U. Behrens³⁰, L. Bellagamba¹⁰, A. Belousov⁵⁴, P. Belov³⁰, A. Bertolin⁶¹, S. Bhadra⁸⁹, M. Bindi¹¹, J.C. Bizot⁵⁸, C. Blohm³⁰, V. Bokhonov^{39,ak}, K. Bondarenko⁴⁰, E.G. Boos², K. Borras³⁰, D. Boscherini¹⁰, D. Bot³⁰, V. Boudry⁶³, I. Bozovic-Jelisavcic⁷, T. Bold³⁶, N. Brümmer¹⁷, J. Bracinik⁹, G. Brandt³⁰, M. Brinkmann³⁰, V. Brisson⁵⁸, D. Britzger³⁰, I. Brock¹², E. Brownson⁴⁹, R. Brugnera⁶², D. Bruncko³⁵, A. Bruni¹⁰, G. Bruni¹⁰, B. Brzozowska⁸⁴, A. Bunyatyan^{33,87}, P.J. Bussey²⁸, A. Bylinkin⁵³, B. Bylsma¹⁷, L. Bystritskaya⁵³, A. Caldwell⁵⁷, A.J. Campbell³⁰, K.B. Cantun Avila⁹⁰, M. Capua¹⁸, R. Carlin⁶², C.D. Catterall⁸⁹, F. Ceccopieri^{4,5}, K. Cerny⁶⁷, V. Cerny³⁵, S. Chekanov⁶, V. Chekelian⁵⁷, J. Chwastowski^{19,o}, J. Ciborowski^{84,aw}, R. Ciesielski^{30,r}, L. Cifarelli¹¹, F. Cindolo¹⁰, A. Contin¹¹, J.G. Contreras⁹⁰, A.M. Cooper-Sarkar⁵⁹, N. Coppola^{30,s}, M. Corradi¹⁰, F. Corriveau⁵², M. Costa⁷⁷, J.A. Coughlan⁶⁰, J. Cvach⁶⁶, G. D'Agostini⁷⁰, J.B. Dainton⁴², F. Dal Corso⁶¹, K. Daum^{86,a,b}, B. Delcourt⁵⁸, J. Delvax^{4,5}, R.K. Dementiev⁵⁶, M. Derrick⁶, R.C.E. Devenish⁵⁹, S. De Pasquale^{11,k}, E.A. De Wolf^{4,5}, J. del Peso⁵⁰, C. Diaconu⁵¹, M. Dobre^{29,g,h}, D. Dobur^{26,ad}, V. Dodonov³³, B.A. Dolgoshein^{55,†}, G. Dolinska⁴⁰, A. Dossanov^{29,57}, A.T. Doyle²⁸, V. Drugakov⁹¹, A. Dubak⁶⁵, L.S. Durkin¹⁷, S. Dusini⁶¹, G. Eckerlin³⁰, S. Egli⁸³, Y. Eisenberg⁶⁸, A. Eliseev⁵⁴, E. Elsen³⁰, P.F. Ermolov^{56,†}, A. Eskreys^{19,†}, S. Fang^{30,t}, L. Favart^{4,5}, S. Fazio¹⁸, A. Fedotov⁵³, R. Felst³⁰, J. Feltesse²⁷, J. Ferencei³⁵, J. Ferrando²⁸, M.I. Ferrero⁷⁷, J. Figiel¹⁹, D.-J. Fischer³⁰, M. Fleischer³⁰, A. Fomenko⁵⁴, M. Forrest^{28,ag}, B. Foster^{59,ao}, E. Gabathuler⁴², G. Gach³⁶, A. Galas¹⁹, E. Gallo²⁴, A. Garfagnini⁶², J. Gayler³⁰, A. Geiser³⁰, S. Ghazaryan³⁰, I. Gialas^{16,ah}, A. Gizhko^{40,am}, L.K. Gladilin^{56,an}, D. Gladkov⁵⁵, C. Glasman⁵⁰, A. Glazov³⁰, L. Goerlich¹⁹, N. Gogitidze⁵⁴, O. Gogota⁴⁰, Y.A. Golubkov⁵⁶, P. Göttlicher^{30,u}, M. Gouzevitch^{30,c}, C. Grab⁹², I. Grabowska-Bold³⁶, A. Grebenyuk³⁰, J. Grebenyuk³⁰, T. Greenshaw⁴², I. Gregor³⁰, G. Grigorescu³, G. Grindhammer⁵⁷, G. Grzelak⁸⁴, O. Gueta⁷², M. Guzik³⁶, C. Gwenlan^{59,ap}, A. Hüttmann³⁰, T. Haas³⁰, S. Habib³⁰, D. Haidt³⁰, W. Hain³⁰, R. Hamatsu⁷⁶, J.C. Hart⁶⁰, H. Hartmann¹², G. Hartner⁸⁹, R.C.W. Henderson⁴¹, E. Hennekemper³², H. Henschel⁹¹, M. Herbst³², G. Herrera⁴⁸, M. Hildebrandt⁸³, E. Hilger¹², K.H. Hiller⁹¹, J. Hladký⁶⁶, D. Hochman⁶⁸, D. Hoffmann⁵¹, R. Hori⁷⁵, R. Horisberger⁸³, T. Hreus^{4,5}, F. Huber³¹, Z.A. Ibrahim³⁷, Y. Iga⁷³, R. Ingber⁷², M. Ishitsuka⁷⁴, M. Jacquet⁵⁸, H.-P. Jakob¹², X. Janssen^{4,5}, F. Januschek³⁰, T.W. Jones⁴⁵, L. Jönsson⁴⁷, M. Jüngst¹², H. Jung^{30,4,5}, I. Kadenko⁴⁰, B. Kahle³⁰, S. Kananov⁷², T. Kanno⁷⁴, M. Kapichine²³, U. Karshon⁶⁸, F. Karstens^{26,ae}, I.I. Katkov^{30,v}, P. Kaur^{15,m}, M. Kaur¹⁵, I.R. Kenyon⁹, A. Keramidas³, L.A. Khein⁵⁶, C. Kiesling⁵⁷, J.Y. Kim³⁸, D. Kisielewska³⁶, S. Kitamura^{76,au}, R. Klanner²⁹, M. Klein⁴², U. Klein^{30,w}, C. Kleinwort³⁰, E. Koffeman³, R. Kogler²⁹, N. Kondrashova^{40,am}, O. Kononenko⁴⁰, P. Kooijman³, I. Korol⁴⁰, I.A. Korzhavina^{56,an}, P. Kostka⁹¹, A. Kotański^{20,p}, U. Kötz³⁰, H. Kowalski³⁰, M. Krämer³⁰, J. Kretzschmar⁴², K. Krüger³², O. Kuprash³⁰, M. Kuze⁷⁴, M.P.J. Landon⁴³, W. Lange⁹¹, G. Laštovička-Medin⁶⁵, P. Laycock⁴², A. Lebedev⁵⁴, A. Lee¹⁷, V. Lendermann³², B.B. Levchenko⁵⁶, S. Levonian³⁰, A. Levy⁷², V. Libov³⁰, S. Limentani⁶², T.Y. Ling¹⁷, K. Lipka^{30,g}, M. Lisovyi³⁰, B. List³⁰, J. List³⁰, E. Lobodzinska³⁰, B. Lobodzinski³⁰, W. Lohmann⁹¹, B. Lühr³⁰, E. Lohrmann²⁹, K.R. Long⁴⁴, A. Longhin^{61,aq}, D. Lontkovskiy³⁰, R. Lopez-Fernandez⁴⁸, V. Lubimov⁵³, O.Y. Lukina⁵⁶, J. Maeda^{74,at}, S. Magill⁶, I. Makarenko³⁰, E. Malinovski⁵⁴, J. Malka³⁰, R. Mankel³⁰, A. Margotti¹⁰, G. Marini⁷⁰, J.F. Martin⁷⁹, H.-U. Martyn¹, A. Mastroberardino¹⁸, M.C.K. Mattingly⁸, S.J. Maxfield⁴², A. Mehta⁴², I.-A. Melzer-Pellmann³⁰, S. Mergelmeyer¹², A.B. Meyer³⁰, H. Meyer⁸⁶, J. Meyer³⁰, S. Miglioranza^{30,x}

S. Mikocki¹⁹, I. Milcewicz-Mika¹⁹, F. Mohamad Idris³⁷, V. Monaco⁷⁷, A. Montanari³⁰, F. Moreau⁶³, A. Morozov²³, J.V. Morris⁶⁰, J.D. Morris^{13,1}, K. Mujkic^{30,y}, K. Müller⁹³, B. Musgrave⁶, K. Nagano⁸⁰, T. Namsoo^{30,z}, R. Nania¹⁰, T. Naumann⁹¹, P.R. Newman⁹, C. Niebuhr³⁰, A. Nigro⁷⁰, D. Nikitin²³, Y. Ning³⁴, T. Nobe⁷⁴, D. Notz³⁰, G. Nowak¹⁹, K. Nowak^{30,g}, R.J. Nowak⁸⁴, A.E. Nuncio-Quiroz¹², B.Y. Oh⁸², N. Okazaki⁷⁵, K. Olkiewicz¹⁹, J.E. Olsson³⁰, Y. Onishchuk⁴⁰, D. Ozerov³⁰, P. Pahl³⁰, V. Palichik²³, M. Pandurovic⁷, K. Papageorgiu¹⁶, A. Parenti³⁰, C. Pascaud⁵⁸, G.D. Patel⁴², E. Paul¹², J.M. Pawlak⁸⁴, B. Pawlik¹⁹, P.G. Pelfer²⁵, A. Pellegrino³, E. Perez^{27,d}, W. Perlański^{84,ax}, H. Perrey³⁰, A. Petrukhin³⁰, I. Picuric⁶⁵, K. Piotrkowski⁴⁶, H. Pirumov³¹, D. Pitzl³⁰, R. Plačákytė^{30,g}, P. Pluciński^{85,ay}, B. Pokorný⁶⁷, N.S. Pokrovskiy², R. Polifka^{67,i}, A. Polini¹⁰, B. Povh³³, A.S. Proskuryakov⁵⁶, M. Przybycień³⁶, V. Radescu^{30,g}, N. Raicevic⁶⁵, A. Raval³⁰, T. Ravdandorj⁸¹, D.D. Reeder⁴⁹, P. Reimer⁶⁶, B. Reisert⁵⁷, Z. Ren³⁴, J. Repond⁶, Y.D. Ri^{76,av}, E. Rizvi⁴³, A. Robertson⁵⁹, P. Robmann⁹³, P. Roloff^{30,x}, R. Roosen^{4,5}, A. Rostovtsev⁵³, M. Rotaru¹⁴, I. Rubinsky³⁰, J.E. Ruiz Tabasco⁹⁰, S. Rusakov⁵⁴, M. Ruspa⁷⁸, R. Sacchi⁷⁷, D. Šálek⁶⁷, U. Samson¹², D.P.C. Sankey⁶⁰, G. Sartorelli¹¹, M. Sauter³¹, E. Sauvan^{51,j}, A.A. Savin⁴⁹, D.H. Saxon²⁸, M. Schioppa¹⁸, S. Schlenstedt⁹¹, P. Schleper²⁹, W.B. Schmidke⁵⁷, S. Schmitt³⁰, U. Schneekloth³⁰, L. Schoeffel²⁷, V. Schönberg¹², A. Schöning³¹, T. Schörner-Sadenius³⁰, H.-C. Schultz-Coulon³², J. Schwartz⁵², F. Sciulli³⁴, F. Sefkow³⁰, L.M. Shcheglova⁵⁶, R. Shehzadi¹², S. Shimizu^{75,x}, L.N. Shtarkov⁵⁴, S. Shushkevich³⁰, I. Singh^{15,m}, I.O. Skillicorn²⁸, W. Słomiński^{20,q}, T. Sloan⁴¹, W.H. Smith⁴⁹, V. Sola²⁹, A. Solano⁷⁷, Y. Soloviev^{26,54}, D. Son²¹, P. Sopicki¹⁹, V. Sosnovtsev⁵⁵, D. South³⁰, V. Spaskov²³, A. Specka⁶³, A. Spiridonov^{30,aa}, H. Stadie²⁹, L. Stanco⁶¹, Z. Staykova^{4,5}, M. Steder³⁰, N. Stefaniuk⁴⁰, B. Stella⁶⁹, A. Stern⁷², T.P. Stewart⁷⁹, A. Stifutkin⁵⁵, G. Stoicea¹⁴, P. Stopa¹⁹, U. Straumann⁹³, S. Suchkov⁵⁵, G. Susinno¹⁸, L. Suszycki³⁶, T. Sykora^{4,5,67}, J. Sztuk-Dambietz²⁹, J. Szuba^{30,ab}, D. Szuba²⁹, A.D. Tapper⁴⁴, E. Tassi^{18,n}, J. Terrón⁵⁰, T. Theedt³⁰, P.D. Thompson⁹, H. Tiecke³, K. Tokushuku^{80,ai}, J. Tomaszewska^{30,ac}, T.H. Tran⁵⁸, D. Traynor⁴³, P. Truöl⁹³, V. Trusov⁴⁰, I. Tsakov⁷¹, B. Tseepeldorj^{81,f}, T. Tsurugai⁸⁸, M. Turcato²⁹, O. Turkot^{40,am}, J. Turnau¹⁹, T. Tymieniecka^{85,az}, M. Vázquez^{3,x}, A. Valkárová⁶⁷, C. Vallée⁵¹, P. Van Mechelen^{4,5}, Y. Vazdik⁵⁴, A. Verbytskyi³⁰, O. Viazlo⁴⁰, N.N. Vlasov^{26,af}, R. Walczak⁵⁹, W.A.T. Wan Abdullah³⁷, D. Wegener²², J.J. Whitmore^{82,ar}, K. Wichmann³⁰, L. Wiggers³, M. Wing⁴⁵, M. Wlasenko¹², G. Wolf³⁰, H. Wolfe⁴⁹, K. Wrona³⁰, E. Wünsch³⁰, A.G. Yagües-Molina³⁰, S. Yamada⁸⁰, Y. Yamazaki^{80,aj}, R. Yoshida⁶, C. Youngman³⁰, O. Zabiegalo^{40,am}, J. Žáček⁶⁷, J. Zálešák⁶⁶, L. Zawiejski¹⁹, O. Zenaiev³⁰, W. Zeuner^{30,x}, Z. Zhang⁵⁸, B.O. Zhautykov², N. Zhmak^{39,ak}, A. Zhokin⁵³, A. Zichichi¹¹, R. Žlebčík⁶⁷, H. Zohrabyan⁸⁷, Z. Zolkapli³⁷, F. Zomer⁵⁸, D.S. Zotkin⁵⁶, A.F. Żarnecki⁸⁴

¹I. Physikalisches Institut der RWTH, Aachen, Germany

²Institute of Physics and Technology of Ministry of Education and Science of Kazakhstan, Almaty, Kazakhstan

³NIKHEF and University of Amsterdam, Amsterdam, Netherlands^{ca}

⁴Inter-University Institute for High Energies ULB-VUB, Brussels, Belgium^{bb}

⁵Universiteit Antwerpen, Antwerpen, Belgium^{bb}

⁶Argonne National Laboratory, Argonne, IL 60439-4815, USA

⁷Vinca Institute of Nuclear Sciences, University of Belgrade, 1100 Belgrade, Serbia

⁸Andrews University, Berrien Springs, MI 49104-0380, USA

⁹School of Physics and Astronomy, University of Birmingham, Birmingham, UK^{bo}

¹⁰INFN Bologna, Bologna, Italy^{bm}

¹¹University and INFN Bologna, Bologna, Italy^{bm}

¹²Physikalisches Institut der Universität Bonn, Bonn, Germany^{bn}

¹³H.H. Wills Physics Laboratory, University of Bristol, Bristol, UK^{bo}

¹⁴National Institute for Physics and Nuclear Engineering (NIPNE), Bucharest, Romania^{bj}

¹⁵Department of Physics, Panjab University, Chandigarh, India

¹⁶Department of Engineering in Management and Finance, Univ. of the Aegean, Chios, Greece

¹⁷Physics Department, Ohio State University, Columbus, OH 43210, USA^{bl}

¹⁸Physics Department and INFN, Calabria University, Cosenza, Italy^{bm}

¹⁹The Henryk Niewodniczanski Institute of Nuclear Physics, Polish Academy of Sciences, Cracow, Poland^{bc}

²⁰Department of Physics, Jagellonian University, Cracow, Poland

²¹Center for High Energy Physics, Kyungpook National University, Daegu, South Korea^{bu}

²²Institut für Physik, TU Dortmund, Dortmund, Germany^{ba}

²³Joint Institute for Nuclear Research, Dubna, Russia

²⁴INFN Florence, Florence, Italy^{bm}

²⁵University and INFN Florence, Florence, Italy^{bm}

- ²⁶Fakultät für Physik der Universität Freiburg i.Br., Freiburg i.Br., Germany
- ²⁷CEA, DSM/Irfu, CE-Saclay, Gif-sur-Yvette, France
- ²⁸School of Physics and Astronomy, University of Glasgow, Glasgow, UK^{bo}
- ²⁹Institut für Experimentalphysik, Universität Hamburg, Hamburg, Germany^{ba,bs}
- ³⁰Deutsches Elektronen-Synchrotron DESY, Hamburg, Germany
- ³¹Physikalisches Institut, Universität Heidelberg, Heidelberg, Germany^{ba}
- ³²Kirchhoff-Institut für Physik, Universität Heidelberg, Heidelberg, Germany^{ba}
- ³³Max-Planck-Institut für Kernphysik, Heidelberg, Germany
- ³⁴Nevis Laboratories, Columbia University, Irvington on Hudson, NY 10027, USA^{bq}
- ³⁵Institute of Experimental Physics, Slovak Academy of Sciences, Košice, Slovak Republic^{bd}
- ³⁶Faculty of Physics and Applied Computer Science, AGH-University of Science and Technology, Krakow, Poland^{br}
- ³⁷Jabatan Fizik, Universiti Malaya, 50603 Kuala Lumpur, Malaysia^{bp}
- ³⁸Institute for Universe and Elementary Particles, Chonnam National University, Kwangju, South Korea
- ³⁹Institute for Nuclear Research, National Academy of Sciences, Kyiv, Ukraine
- ⁴⁰Department of Nuclear Physics, National Taras Shevchenko University of Kyiv, Kyiv, Ukraine
- ⁴¹Department of Physics, University of Lancaster, Lancaster, UK^{bo}
- ⁴²Department of Physics, University of Liverpool, Liverpool, UK^{bo}
- ⁴³School of Physics and Astronomy, Queen Mary, University of London, London, UK^{bo}
- ⁴⁴High Energy Nuclear Physics Group, Imperial College London, London, UK^{bo}
- ⁴⁵Physics and Astronomy Department, University College London, London, UK^{bo}
- ⁴⁶Institut de Physique Nucléaire, Université Catholique de Louvain, Louvain-la-Neuve, Belgium^{bv}
- ⁴⁷Physics Department, University of Lund, Lund, Sweden^{bc}
- ⁴⁸Departamento de Física, CINVESTAV IPN, México City, México^{bh}
- ⁴⁹Department of Physics, University of Wisconsin, Madison, WI 53706, USA^{bl}
- ⁵⁰Departamento de Física Teórica, Universidad Autónoma de Madrid, Madrid, Spain^{bw}
- ⁵¹CPM, Aix-Marseille Univ, CNRS/IN2P3, 13288 Marseille, France
- ⁵²Department of Physics, McGill University, Montréal, Québec H3A 2T8, Canada^{bx}
- ⁵³Institute for Theoretical and Experimental Physics, Moscow, Russia^{bi}
- ⁵⁴Lebedev Physical Institute, Moscow, Russia
- ⁵⁵Moscow Engineering Physics Institute, Moscow, Russia^{by}
- ⁵⁶Skobeltsyn Institute of Nuclear Physics, Lomonosov Moscow State University, Moscow, Russia^{bz}
- ⁵⁷Max-Planck-Institut für Physik, Munich, Germany
- ⁵⁸LAL, Université Paris-Sud, CNRS/IN2P3, Orsay, France
- ⁵⁹Department of Physics, University of Oxford, Oxford, UK^{bo}
- ⁶⁰STFC, Rutherford Appleton Laboratory, Didcot, Oxfordshire, UK^{bo}
- ⁶¹INFN Padova, Padova, Italy^{bm}
- ⁶²Dipartimento di Fisica dell' Università and INFN, Padova, Italy^{bm}
- ⁶³LLR, Ecole Polytechnique, CNRS/IN2P3, Palaiseau, France
- ⁶⁴LPNHE, Université Pierre et Marie Curie Paris 6, Université Denis Diderot Paris 7, CNRS/IN2P3, Paris, France
- ⁶⁵Faculty of Science, University of Montenegro, Podgorica, Montenegro^{bk}
- ⁶⁶Institute of Physics of the Academy of Sciences of the Czech Republic, Praha, Czech Republic^{bf}
- ⁶⁷Faculty of Mathematics and Physics of Charles University, Praha, Czech Republic^{bf}
- ⁶⁸Department of Particle Physics and Astrophysics, Weizmann Institute, Rehovot, Israel
- ⁶⁹Dipartimento di Fisica, Università di Roma Tre and INFN Roma 3, Rome, Italy
- ⁷⁰Dipartimento di Fisica, Università 'La Sapienza' and INFN, Rome, Italy^{bm}
- ⁷¹Institute for Nuclear Research and Nuclear Energy, Sofia, Bulgaria
- ⁷²Raymond and Beverly Sackler Faculty of Exact Sciences, School of Physics, Tel Aviv University, Tel Aviv, Israel^{cb}
- ⁷³Polytechnic University, Tokyo, Japan^{bt}
- ⁷⁴Department of Physics, Tokyo Institute of Technology, Tokyo, Japan^{bt}
- ⁷⁵Department of Physics, University of Tokyo, Tokyo, Japan^{bt}
- ⁷⁶Department of Physics, Tokyo Metropolitan University, Tokyo, Japan^{bt}
- ⁷⁷Università di Torino and INFN, Torino, Italy^{bm}
- ⁷⁸Università del Piemonte Orientale, Novara, and INFN, Torino, Italy^{bm}
- ⁷⁹Department of Physics, University of Toronto, Toronto, Ontario M5S 1A7, Canada^{bx}
- ⁸⁰Institute of Particle and Nuclear Studies, KEK, Tsukuba, Japan^{bt}
- ⁸¹Institute of Physics and Technology of the Mongolian Academy of Sciences, Ulaanbaatar, Mongolia
- ⁸²Department of Physics, Pennsylvania State University, University Park, PA 16802, USA^{bq}
- ⁸³Paul Scherrer Institut, Villigen, Switzerland
- ⁸⁴Faculty of Physics, University of Warsaw, Warsaw, Poland
- ⁸⁵National Centre for Nuclear Research, Warsaw, Poland
- ⁸⁶Fachbereich C, Universität Wuppertal, Wuppertal, Germany
- ⁸⁷Yerevan Physics Institute, Yerevan, Armenia
- ⁸⁸Faculty of General Education, Meiji Gakuin University, Yokohama, Japan^{bt}
- ⁸⁹Department of Physics, York University, Toronto, Ontario M3J 1P3, Canada^{bx}
- ⁹⁰Departamento de Física Aplicada, CINVESTAV, Mérida, Yucatán, México^{bh}

⁹¹Deutsches Elektronen-Synchrotron DESY, Zeuthen, Germany

⁹²Institut für Teilchenphysik, ETH, Zurich, Switzerland^{bg}

⁹³Physik-Institut der Universität Zürich, Zurich, Switzerland^{bg}

Received: 20 July 2012 / Revised: 24 September 2012 / Published online: 10 October 2012

© The Author(s) 2012. This article is published with open access at Springerlink.com

Abstract A combination of the inclusive diffractive cross section measurements made by the H1 and ZEUS Collaborations at HERA is presented. The analysis uses samples of diffractive deep inelastic ep scattering data at a centre-of-mass energy $\sqrt{s} = 318$ GeV where leading protons are detected by dedicated spectrometers. Correlations of systematic uncertainties are taken into account, resulting in an

improved precision of the cross section measurement which reaches 6 % for the most precise points. The combined data cover the range $2.5 < Q^2 < 200$ GeV² in photon virtuality, $0.00035 < x_{\mathbb{P}} < 0.09$ in proton fractional momentum loss, $0.09 < |t| < 0.55$ GeV² in squared four-momentum transfer at the proton vertex and $0.0018 < \beta < 0.816$ in $\beta = x/x_{\mathbb{P}}$, where x is the Bjorken scaling variable.

^ae-mail: daum@mail.desy.de

^bAlso at Rechenzentrum, Universität Wuppertal, Wuppertal, Germany.

^cAlso at IPNL, Université Claude Bernard Lyon 1, CNRS/IN2P3, Villeurbanne, France.

^dAlso at CERN, Geneva, Switzerland.

^eAlso at Faculty of Physics, University of Bucharest, Bucharest, Romania.

^fAlso at Ulaanbaatar University, Ulaanbaatar, Mongolia.

^gSupported by the Initiative and Networking Fund of the Helmholtz Association (HGF) under the contract VH-NG-401 and S0-072.

^hAbsent on leave from NIPNE-HH, Bucharest, Romania.

ⁱAlso at Department of Physics, University of Toronto, Toronto, Ontario, Canada M5S 1A7.

^jAlso at LAPP, Université de Savoie, CNRS/IN2P3, Annecy-le-Vieux, France.

^kNow at University of Salerno, Italy.

^lNow at Queen Mary University of London, UK.

^mAlso funded by Max Planck Institute for Physics, Munich, Germany.

ⁿAlso Senior Alexander von Humboldt Research Fellow at Hamburg University, Institute of Experimental Physics, Hamburg, Germany.

^oAlso at Cracow University of Technology, Faculty of Physics, Mathematics and Applied Computer Science, Poland.

^pSupported by the research grant No. 1 P03B 04529 (2005-2008).

^qSupported by the Polish National Science Centre, project No. DEC-2011/01/BST2/03643.

^rNow at Rockefeller University, New York, NY 10065, USA.

^sNow at DESY group FS-CFEL-1.

^tNow at Institute of High Energy Physics, Beijing, China.

^uNow at DESY group FEB, Hamburg, Germany.

^vAlso at Moscow State University, Russia.

^wNow at University of Liverpool, UK.

^xNow at CERN, Geneva, Switzerland.

^yAlso affiliated with University College London, UK.

^zNow at Goldman Sachs, London, UK.

^{aa}Also at Institute of Theoretical and Experimental Physics, Moscow, Russia.

^{ab}Also at FPACS, AGH-UST, Cracow, Poland.

^{ac}Partially supported by Warsaw University, Poland.

^{ad}Now at Istituto Nucleare di Fisica Nazionale (INFN), Pisa, Italy.

^{ae}Now at Haase Energie Technik AG, Neumünster, Germany.

^{af}Now at Department of Physics, University of Bonn, Germany.

^{ag}Now at Biodiversität und Klimaforschungszentrum (BiK-F), Frankfurt, Germany.

^{ah}Also affiliated with DESY, Germany.

^{ai}Also at University of Tokyo, Japan.

^{aj}Now at Kobe University, Japan.

^{ak}Supported by DESY, Germany.

^{al}Member of National Technical University of Ukraine, Kyiv Polytechnic Institute, Kyiv, Ukraine.

^{am}Member of National University of Kyiv—Mohyla Academy, Kyiv, Ukraine.

^{an}Partly supported by the Russian Foundation for Basic Research, grant 11-02-91345-DFG_a.

^{ao}Alexander von Humboldt Professor; also at DESY and University of Oxford.

^{ap}STFC Advanced Fellow.

^{aq}Now at LNF, Frascati, Italy.

^{ar}This material was based on work supported by the National Science Foundation, while working at the Foundation.

^{as}Also at Max Planck Institute for Physics, Munich, Germany, External Scientific Member.

^{at}Now at Tokyo Metropolitan University, Japan.

^{au}Now at Nihon Institute of Medical Science, Japan.

^{av}Now at Osaka University, Osaka, Japan.

^{aw}Also at Lodz University, Poland.

^{ax}Member of Lodz University, Poland.

^{ay}Now at Department of Physics, Stockholm University, Stockholm, Sweden.

^{az}Also at Cardinal Stefan Wyszyński University, Warsaw, Poland.

^{ba}Supported by the Bundesministerium für Bildung und Forschung, FRG, under contract numbers 05H09GUF, 05H09VHC, 05H09VHF, 05H16PEA.

^{bb}Supported by FNRS-FWO-Vlaanderen, IISN-IIKW and IWT and by Interuniversity Attraction Poles Programme, Belgian Science Policy.

^{bc}Supported by Polish Ministry of Science and Higher Education, grants DPN/N168/DESY/2009 and DPN/N188/DESY/2009.

1 Introduction

Diffractive collisions in deep inelastic electron-proton scattering (DIS), $ep \rightarrow eXp$, where the proton in the final state carries most of the beam momentum and X represents all other final state particles, have been studied extensively at the HERA collider. They can be viewed as resulting from processes in which a photon exchanged between the electron and the proton probes a colour-singlet combination of partons with vacuum quantum numbers emitted by the proton. The negative four-momentum squared of the virtual photon, Q^2 , supplies a hard scale, which allows the application of perturbative quantum chromodynamics (QCD). Diffractive reactions in DIS are a tool to investigate low-momentum partons in the proton, notably through the study of diffractive parton distribution functions (DPDFs), determined by a QCD analysis of the data.

In diffractive ep scattering the virtual photon dissociates at a photon-proton centre-of-mass energy W and squared four-momentum transfer t at the proton vertex (Fig. 1), producing a hadronic system X with mass M_X . The fractional longitudinal momentum loss of the proton is denoted as $x_{\mathbb{P}}$, while the fraction of this momentum taking part in the interaction with the photon is denoted as β . These variables are related to Bjorken x by $x = \beta x_{\mathbb{P}}$. The variable β is related to M_X , t and Q^2 by $\beta = Q^2 / (Q^2 + M_X^2 - t)$. The variable $x_{\mathbb{P}}$ is given by $x_{\mathbb{P}} = (Q^2 + M_X^2 - t) / (Q^2 + W^2 - m_p^2)$, where

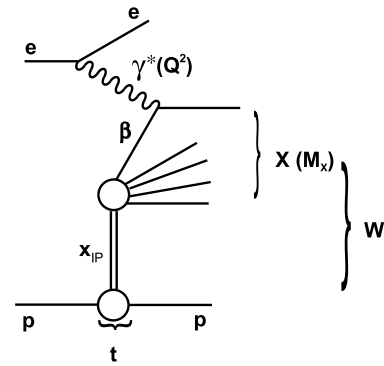


Fig. 1 Diagram of the reaction $ep \rightarrow eXp$

m_p is the proton mass. The variables W , Q^2 and the fractional energy loss y of the electron in the proton rest frame are related by $W^2 \simeq sy - Q^2$, where s is the square of the ep centre-of-mass energy.

Similarly to inclusive DIS, diffractive cross section measurements are conventionally expressed in terms of the reduced diffractive cross section, $\sigma_r^{D(4)}$, which is related to the measured ep cross section by

$$\frac{d\sigma^{ep \rightarrow eXp}}{d\beta dQ^2 dx_{\mathbb{P}} dt} = \frac{4\pi\alpha^2}{\beta Q^4} \left[1 - y + \frac{y^2}{2} \right] \times \sigma_r^{D(4)}(\beta, Q^2, x_{\mathbb{P}}, t). \tag{1}$$

The reduced cross section $\sigma_r^{D(3)}(\beta, Q^2, x_{\mathbb{P}})$ is obtained by

^{bd}Supported by VEGA SR grant no. 2/7062/27.

^{be}Supported by the Swedish Natural Science Research Council.

^{bf}Supported by the Ministry of Education of the Czech Republic under the projects LC527, INGO-LA09042 and MSM0021620859.

^{bg}Supported by the Swiss National Science Foundation.

^{bh}Supported by CONACYT, México, grant 48778-F.

^{bi}Russian Foundation for Basic Research (RFBR), grant no. 1329.2008.2 and Rosatom.

^{bj}Supported by the Romanian National Authority for Scientific Research under the contract PN 09370101.

^{bk}Partially Supported by Ministry of Science of Montenegro, no. 05-1/3-3352.

^{bl}Supported by the US Department of Energy.

^{bm}Supported by the Italian National Institute for Nuclear Physics (INFN).

^{bn}Supported by the German Federal Ministry for Education and Research (BMBF), under contract No. 05 H09PDF.

^{bo}Supported by the Science and Technology Facilities Council, UK.

^{bp}Supported by an FRGS grant from the Malaysian government.

^{bq}Supported by the US National Science Foundation. Any opinion, findings and conclusions or recommendations expressed in this material are those of the authors and do not necessarily reflect the views of the National Science Foundation.

^{br}Supported by the Polish Ministry of Science and Higher Education and its grants for Scientific Research.

^{bs}Supported by the German Federal Ministry for Education and Research (BMBF), under contract No. 05h09GUF, and the SFB 676 of the Deutsche Forschungsgemeinschaft (DFG).

^{bt}Supported by the Japanese Ministry of Education, Culture, Sports, Science and Technology (MEXT) and its grants for Scientific Research.

^{bu}Supported by the Korean Ministry of Education and Korea Science and Engineering Foundation.

^{bv}Supported by FNRS and its associated funds (IISN and FRIA) and by an Inter-University Attraction Poles Programme subsidised by the Belgian Federal Science Policy Office.

^{bw}Supported by the Spanish Ministry of Education and Science through funds provided by CICYT.

^{bx}Supported by the Natural Sciences and Engineering Research Council of Canada (NSERC).

^{by}Partially supported by the German Federal Ministry for Education and Research (BMBF).

^{bz}Supported by RF Presidential grant N 4142.2010.2 for Leading Scientific Schools, by the Russian Ministry of Education and Science through its grant for Scientific Research on High Energy Physics and under contract No. 02.740.11.0244.

^{ca}Supported by the Netherlands Foundation for Research on Matter (FOM).

^{cb}Supported by the Israel Science Foundation.

[†]Deceased.

integrating $\sigma_r^{D(4)}(\beta, Q^2, x_{\mathbb{P}}, t)$ over t . The diffractive reduced cross section is related to the diffractive structure functions by:

$$\begin{aligned} \sigma_r^{D(3)}(x_{\mathbb{P}}, \beta, Q^2, y) \\ = F_2^{D(3)}(x_{\mathbb{P}}, \beta, Q^2) - \frac{y^2}{1 + (1 - y)^2} F_L^{D(3)}(x_{\mathbb{P}}, \beta, Q^2). \end{aligned} \quad (2)$$

Experimentally, diffractive ep scattering is characterised by the presence of a leading proton in the final state and by a depletion of hadronic activity in the pseudo-rapidity¹ distribution of particles (large rapidity gap, LRG) in the forward (proton) direction. Both of these signatures have been exploited in various analyses by H1 and ZEUS to select diffractive samples either by tagging the outgoing proton in dedicated proton spectrometers [1–4] or by requiring the presence of a large rapidity gap [4–6]. The two methods differ partially in the accessible kinematic ranges (lower $x_{\mathbb{P}}$ reach for the LRG data) and substantially in their dominant sources of systematic uncertainties. In LRG-based measurements, the largest uncertainty arises from proton dissociative events, $ep \rightarrow eXN$, in which the proton dissociates into a low mass state N . Low $x_{\mathbb{P}}$ samples selected by the proton spectrometers have little or no proton dissociation contribution, but their precision is limited statistically by the small acceptances and systematically by large uncertainties in the proton tagging efficiency, which strongly depends on the proton-beam optics. The results from both methods are found to be consistent [1, 2, 4, 6, 7].

Combining measurements can provide more precise and kinematically extended data than the individual measurements. In this paper, a combination of the H1 [1, 2] and the ZEUS [3, 4] proton spectrometer results is presented. The combination is performed using the weighted averaging method introduced in [8] and extended in [9, 10]. The correlated systematic uncertainties and global normalisations are constrained in the fit such that one consistent data set is obtained. Since H1 and ZEUS have employed different experimental techniques, using different detectors and methods of kinematic reconstruction, the combination leads to significantly reduced uncertainties. The kinematic range of the combined data is: $2.5 \leq Q^2 \leq 200 \text{ GeV}^2$, $0.0018 \leq \beta \leq 0.816$, $0.00035 \leq x_{\mathbb{P}} \leq 0.09$ and $0.09 < |t| < 0.55 \text{ GeV}^2$. The latter range restricts the analysis to the t values directly accessible by both the H1 and ZEUS proton spectrometers.

¹The pseudo-rapidity is defined as $\eta = -\ln \tan \theta/2$ where the polar angle θ is measured with respect to the proton beam direction.

2 Combination of the H1 and ZEUS measurements

2.1 Data samples

The H1 [11–13] and ZEUS [14] detectors were general purpose instruments which consisted of tracking systems surrounded by electromagnetic and hadronic calorimeters and muon detectors, ensuring close to 4π coverage about the ep interaction point. Both detectors were equipped with proton spectrometers; the Leading Proton Spectrometer (LPS) for ZEUS, the Forward Proton Spectrometer (FPS) and the Very Forward Proton Spectrometer (VFPS) for H1. The LPS and FPS spectrometers were located between 60 and 90 m away from the main detectors in the forward (proton beam) direction. The VFPS spectrometer was located around 220 m away from the main H1 detector in the forward direction.

The combination is based on the cross sections measured with the H1 FPS [1, 2] and the ZEUS LPS [3, 4]. The bulk of the data [1, 2, 4] was taken at electron and proton beam energies of $E_e \simeq 27.5 \text{ GeV}$ and $E_p = 920 \text{ GeV}$, respectively, corresponding to an ep centre-of-mass energy of $\sqrt{s} = 318 \text{ GeV}$. The earlier ZEUS LPS data [3] collected at $E_p = 820 \text{ GeV}$ are corrected to a common $\sqrt{s} = 318 \text{ GeV}$ by using the extrapolation procedure described in Sect. 2.1.2. The three-fold differential reduced cross sections, $\sigma_r^{D(3)}(\beta, Q^2, x_{\mathbb{P}})$, are combined. For the original measurements, the main H1 and ZEUS detectors are used to reconstruct Q^2 , W and x , whereas M_X , β , $x_{\mathbb{P}}$ and t are derived from the proton spectrometer measurements or from combined information of the proton spectrometers and the main detectors. In Table 1 the data sets used for the combination are listed together with their kinematic ranges and integrated luminosities.

2.1.1 Restricted t range

In the individual analyses [1–4] the reduced cross sections are directly measured for ranges of the squared four-momentum transfer t visible to the proton spectrometers (see Table 1) and extrapolated to the range² $|t_{\min}| < |t| < 1 \text{ GeV}^2$ (denoted in the following as ‘the full t range’), assuming an exponential t dependence of the diffractive cross section and using the exponential slope measured from the data. Due to the uncertainties of the slope parameters measured by H1 [1, 2] and ZEUS [3, 4], this extrapolation introduces an additional uncertainty in the normalisation of the cross section. To reduce this source of systematic uncertainty, the H1 and ZEUS cross sections are combined in the restricted t range $0.09 < |t| < 0.55 \text{ GeV}^2$ covered by the proton spectrometer acceptances of both detectors for

²The smallest kinematically accessible value of $|t|$ is denoted as $|t_{\min}|$.

Table 1 H1 and ZEUS data sets used for the combination of the measurements

Data Set	Q^2 range [GeV ²]	$x_{\mathbb{P}}$ range	y range	β range	t range [GeV ²]	Luminosity [pb ⁻¹]	Ref.
H1 FPS HERA II	4–700	<0.1	0.03–0.8	0.001–1	0.1–0.7	156.6	[2]
H1 FPS HERA I	2–50	<0.1	0.02–0.6	0.004–1	0.08–0.5	28.4	[1]
			W range [GeV]	M_X range [GeV]			
ZEUS LPS 2	2.5–120	0.0002–0.1	40–240	2–40	0.09–0.55	32.6	[4]
ZEUS LPS 1	2–100	<0.1	25–240	> 1.5	0.075–0.35	3.6	[3]

the bulk of the data. The correction factors from the visible t range of the ‘FPS HERA I’ and ‘LPS 1’ data samples to the restricted t range are evaluated by using the t dependencies as a function of $x_{\mathbb{P}}$ measured for each sample. The correction factors for the most precise ‘FPS HERA II’ data are applied in bins of β , Q^2 and $x_{\mathbb{P}}$. For the ‘LPS 2’ sample the restricted range coincides with the visible range. Because of the uncertainty on the exponential slope parameter, such factors introduce uncertainties of 2.2 %, 1.1 % and 5 % on the ‘FPS HERA II’, ‘FPS HERA I’ and ‘LPS 1’ data, respectively, which are included in the normalisation uncertainty on each sample. The total normalisation uncertainties of the data samples are listed in Table 2. In the restricted t range, these uncertainties are in general smaller and the average normalisations are in better agreement than in the full t range; the ratio of the ‘FPS HERA II’ to the ‘LPS 2’ data averaged over the measured data points, which is 0.85 ± 0.01 (stat) ± 0.03 (sys) $^{+0.09}_{-0.12}$ (norm) in the full t range [2], becomes 0.91 ± 0.01 (stat) ± 0.03 (sys) ± 0.08 (norm) in the restricted t range. Within the uncertainties, the ratio does not show any significant β , Q^2 or $x_{\mathbb{P}}$ dependence.

2.1.2 Extrapolation to a common (Q^2 , $x_{\mathbb{P}}$, β) grid

The original binning schemes of the $\sigma_r^{D(3)}$ measurements are very different for H1 and ZEUS. In the H1 case the measurements are extracted at fixed β , whereas for ZEUS the cross section is measured at fixed M_X ; also the Q^2 and $x_{\mathbb{P}}$ central values differ. Therefore, prior to the combination, the H1 and ZEUS data are transformed to a common grid of

Table 2 Normalisation uncertainties in the full range $|t| < 1$ GeV² and in the restricted t range for the data used for the combination of the measurements

Data Set	$ t_{\min} < t < 1$ GeV ²	$0.09 < t < 0.55$ GeV ²
FPS HERA II	± 6 %	± 5 %
FPS HERA I	± 10 %	± 10 %
LPS 2	+11 %, –7 %	± 7 %
LPS 1	+12 %, –10 %	± 11 %

(β , Q^2 , $x_{\mathbb{P}}$) points. The grid points are based on the original binning scheme of the ‘FPS HERA II’ data. The (Q^2 , $x_{\mathbb{P}}$) grid points at the lowest Q^2 value of 2.5 GeV² and at the lowest and highest $x_{\mathbb{P}}$ values, which are beyond the ‘FPS HERA II’ data grid, are taken from the ‘LPS 2’ measurement.

The transformation of a measurement from the original i th point (β_i , Q_i^2 , $x_{\mathbb{P}i}$) to the nearest grid point (β_{grid} , Q_{grid}^2 , $x_{\mathbb{P}\text{grid}}$) is performed by multiplying the measured cross section by the ratio $\sigma_r^{D(3)}(\beta_{\text{grid}}, Q_{\text{grid}}^2, x_{\mathbb{P}\text{grid}})/\sigma_r^{D(3)}(\beta_i, Q_i^2, x_{\mathbb{P}i})$ calculated with the Next-to-Leading-Order (NLO) DPDF ‘ZEUS SJ’ parameterisation [15]. Most of the corrections are smaller than 10 %, while a few points undergo corrections up to ~ 30 %. The procedure is checked by using the NLO DPDF ‘H1 Fit B’ parameterisation [5]. The resulting difference is treated as a procedural uncertainty on the combined cross section, as discussed in Sect. 2.3.2.

The cross sections from all the data sets are shown in Fig. 2 after correcting to $0.09 < |t| < 0.55$ GeV² and transforming to the common grid.

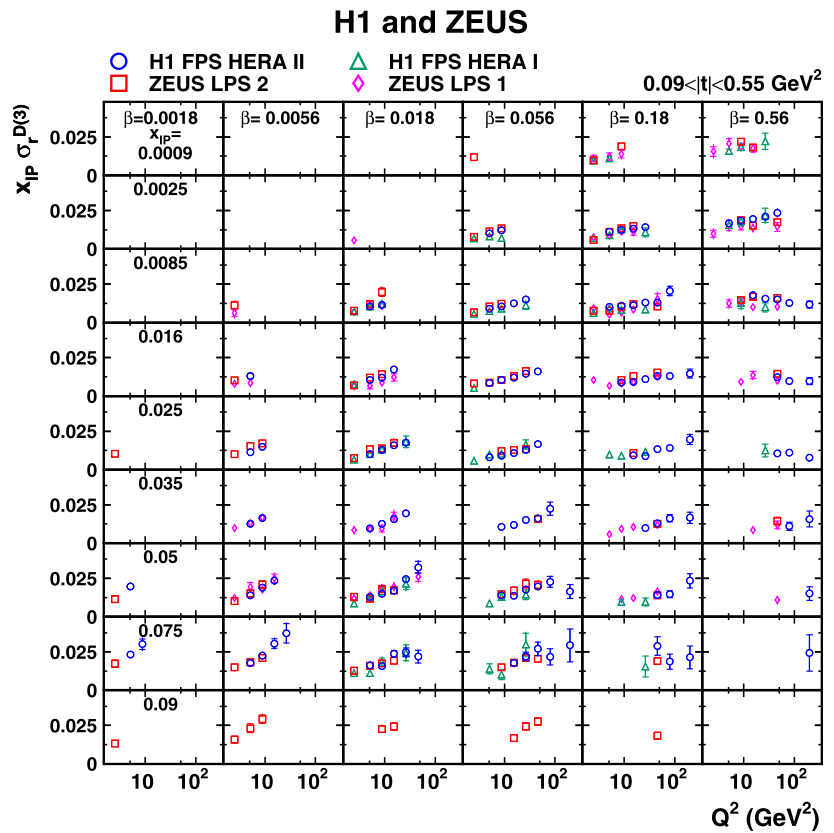
2.2 Combination method

The combination is based on the χ^2 minimisation method described in [8] and used for previous combined HERA results [10]. The averaging procedure is based on the assumption that at a given kinematic point the H1 and ZEUS experiments are measuring the same cross section. The correlated systematic uncertainties are floated coherently. The procedure allows a model independent check of the data consistency and leads to a significant reduction of the correlated uncertainties.

For an individual data set, the χ^2 function is defined as:

$$\chi_{\text{exp}}^2(\mathbf{m}, \mathbf{b}) = \sum_i \frac{[m^i - \sum_j \gamma_j^i m^i b_j - \mu^i]^2}{\delta_{i,\text{stat}}^2 \mu^i (m^i - \sum_j \gamma_j^i m^i b_j) + (\delta_{i,\text{uncor}} m^i)^2} + \sum_j b_j^2 \tag{3}$$

Fig. 2 Reduced diffractive cross section $x_{\mathbb{P}} \sigma_r^{D(3)}(\beta, Q^2, x_{\mathbb{P}})$ for $0.09 < |t| < 0.55 \text{ GeV}^2$ as a function of Q^2 for different values of β and $x_{\mathbb{P}}$. The H1 ‘FPS HERA II’ [2], H1 ‘FPS HERA I’ [1], ZEUS ‘LPS 2’ [4] and ZEUS ‘LPS 1’ [3] data are presented. The *inner error bars* indicate the statistical uncertainties, while the *outer error bars* show the statistical and systematic uncertainties added in quadrature. Normalisation uncertainties are not included in the *error bars* of the individual measurements



Here μ^i is the measured cross section value at a point i ($\beta_i, Q_i^2, x_{\mathbb{P}i}$), and $\gamma_j^i, \delta_{i,\text{stat}}$ and $\delta_{i,\text{uncor}}$ are the relative correlated systematic, relative statistical and relative uncorrelated systematic uncertainties, respectively. The vector m of quantities m^i expresses the values of the combined cross section for each point i and the vector b of quantities b_j expresses the shifts of the correlated systematic uncertainty sources, j , in units of the standard deviation. The relative uncertainties γ_j^i and $\delta_{i,\text{uncor}}$ are multiplied by the combined cross section m^i in order to take into account the fact that the correlated and uncorrelated systematic uncertainties are to a good approximation proportional to the central values (multiplicative uncertainties). On the other hand, the statistical uncertainties scale with the square root of the expected number of events, which is determined by the expected cross section, corrected for the biases due to the correlated systematic uncertainties. This is taken into account by the $\delta_{i,\text{stat}}^2 \mu^i (m^i - \sum_j \gamma_j^i m^i b_j)$ term.

If several analyses provide measurements at the same ($\beta, Q^2, x_{\mathbb{P}}$) values, a χ_{tot}^2 is built [9] from the sum of the χ_{exp}^2 of each data set, assuming the individual data sets to be statistically uncorrelated. The χ_{tot}^2 is minimised with respect to the m^i and b_j from each data set with an iterative procedure. The ratio $\chi_{\text{min}}^2/n_{\text{dof}}$ is a measure of the consistency of the data sets. The number of degrees of freedom, n_{dof} ,

is calculated as the difference between the total number of measurements and the number of averaged points. The uncertainties of the combined cross sections are evaluated from the $\chi_{\text{min}}^2 + 1$ criteria [8–10]. For some of the ($\beta, Q^2, x_{\mathbb{P}}$) points there is only one measurement; however, because of the systematic uncertainty correlations such measurements may be shifted with respect to the original values, and the uncertainties may be reduced.

2.3 Uncertainties

2.3.1 Experimental systematic uncertainties and their correlations

The input cross sections are published with their statistical and systematic uncertainties. The statistical uncertainties correspond to $\delta_{i,\text{stat}}$ in Eq. (3). The systematic uncertainties are classified as point-to-point correlated or point-to-point uncorrelated, corresponding to γ_j^i and $\delta_{i,\text{uncor}}$ respectively, according to the information provided in the corresponding publications, as follows:

- For the two older analyses, ‘FPS HERA I’ and ‘LPS 1’, only the total systematic uncertainties are given [1, 3], with no information on the single contributions and point-to-point correlations. For these two samples only the normalisation uncertainties (Table 2) are considered among

- the correlated systematics, while the remaining uncertainties are treated as uncorrelated.
- For the sample ‘FPS HERA II’ all the systematic sources discussed in [2] are treated as point-to-point correlated. The hadronic energy scale uncertainty is taken as correlated separately for $x_{\mathbb{P}} < 0.012$ and $x_{\mathbb{P}} > 0.012$. This is to account for the different sensitivity to this systematic source for the two $x_{\mathbb{P}}$ regions, where different methods are used to reconstruct the variable β , which are typically sensitive to different regions of the H1 central calorimeter. For $x_{\mathbb{P}} < 0.012$, where the mass M_X of the hadronic final state is used to reconstruct β , the effect on the cross section due to the hadronic energy scale uncertainty is 4 % on average and reaches 6.7 %. For $x_{\mathbb{P}} > 0.012$, where β is reconstructed with the leading proton energy measured by the FPS, the cross section shows almost no sensitivity to the hadronic energy scale.
 - In the ‘LPS 2’ case, the total systematic uncertainties quoted in [4] are decomposed in correlated and uncorrelated following the prescriptions in [15]. They are symmetrised by taking the average of the positive and negative uncertainties.

In the H1 ‘FPS HERA II’ analysis, the systematic effects related to the leading proton measurement are considered as

correlated and derived from the variation of the acceptance in the $x_{\mathbb{P}}$ and t bins when shifting the FPS energy scale and transverse momentum within the estimated uncertainties [2]. In the ZEUS ‘LPS 2’ case, the systematic uncertainty related to the leading proton measurement is dominated by the incomplete knowledge of the beam optics, of the position of the beamline aperture limitations and of the intrinsic transverse-momentum spread of the proton beam at the interaction point. The beam optics contribution is largely independent of the kinematic variables and therefore is taken as a normalisation uncertainty [4]. The other contributions are quantified by varying the cut on the distance of closest approach of the reconstructed proton track to the beampipe, and the value of the intrinsic transverse-momentum spread assumed in the simulation. They are treated as uncorrelated uncertainties.

All the H1 systematic uncertainties are treated as independent of the ZEUS uncertainties, and vice versa. Possible effects due to correlations between the two experiments are taken into account in the procedural uncertainties, discussed in Sect. 2.3.2. In total, 23 independent sources of correlated systematic uncertainties are considered, including the global normalisation for each sample. The full list is given in Table 3.

Table 3 Sources of point-to-point correlated systematic uncertainties considered in the combination. For each source the shifts resulting from the combination in units of the original uncertainty and the values of the final uncertainties as percentages of the original are given

Source	Shift (σ units)	Reduction factor %
FPS HERA II hadronic energy scale $x_{\mathbb{P}} < 0.012$	-1.61	56.9
FPS HERA II hadronic energy scale $x_{\mathbb{P}} > 0.012$	0.13	99.8
FPS HERA II electromagnetic energy scale	0.49	85.9
FPS HERA II electron angle	0.67	66.6
FPS HERA II β reweighting	0.15	90.4
FPS HERA II $x_{\mathbb{P}}$ reweighting	0.05	98.3
FPS HERA II t reweighting	0.70	79.8
FPS HERA II Q^2 reweighting	0.09	97.6
FPS HERA II proton energy	0.05	45.6
FPS HERA II proton p_x	0.62	74.5
FPS HERA II proton p_y	0.27	86.5
FPS HERA II vertex reconstruction	0.07	97.0
FPS HERA II background subtraction	0.84	89.9
FPS HERA II bin centre corrections	-1.05	87.3
FPS HERA II global normalisation	-0.39	84.4
FPS HERA I global normalisation	0.81	48.9
LPS 2 hadronic energy scale	-0.02	55.0
LPS 2 electromagnetic energy scale	-0.14	62.4
LPS 2 $x_{\mathbb{P}}$ reweighting	-0.32	98.2
LPS 2 t reweighting	-0.26	86.4
LPS 2 background subtraction	0.40	94.9
LPS 2 global normalisation	-0.53	67.7
LPS 1 global normalisation	0.86	44.1

2.3.2 Procedural uncertainties

The following uncertainties on the combined cross sections due to the combination procedure are studied:

- The χ^2 function given by Eq. (3) treats all systematic uncertainties as multiplicative, i.e. proportional to the expected central values. While this generally holds for the normalisation uncertainties, it may not be the case for the other uncertainties. To study the sensitivity of the average result to this issue, an alternative averaging is performed. Only the normalisation uncertainty and those related to the t reconstruction (the uncertainties on the ‘FPS HERA II’ proton p_x , p_y reconstruction and on the ‘FPS HERA II’ and ‘LPS 2’ t reweighting) which, for the reasons explained in Sect. 2.1.1, can affect the normalisation, are taken as multiplicative, while all other uncertainties are treated as additive. The difference between this average and the nominal result is of the order of 1 % on average and 6.4 % at most.
- The H1 and ZEUS experiments use similar methods for detector calibration, apply similar reweighting to the Monte Carlo models used for the acceptance corrections and employ similar Monte Carlo models for QED radiative corrections, for the hadronic final state simulation and for background subtraction. Such similarities may lead to correlations between the measurements of the two experiments. Three systematic source are identified as the most likely to be correlated between the two experiments. These are the electromagnetic energy scale and the reweighting of the simulation in $x_{\mathbb{P}}$ and t . Averages are formed for each of the 2^3 possible assumptions on the presence of correlations of these systematic uncertainties between the experiments and are compared with the nominal average for which all sources are assumed to be uncorrelated. The maximum difference between the nominal and the alternative averages is taken as an uncertainty. It is 1.4 % on average and 6.6 % at most, with no particular dependence on the kinematics.
- The bias introduced by transforming the data to the common grid (see Sect. 2.1.2) is studied by using correction factors obtained from the NLO DPDF ‘H1 Fit B’ [5] parameterisation. For a few bins this changes the result by up to 8 %, but the average effect is 1.2 %.
- The averaging procedure shifts the H1 hadronic energy scale at $x_{\mathbb{P}} < 0.012$ by substantially more than 1σ of the nominal value (see Sect. 3). To study the sensitivity of the average result to the treatment of the uncertainty on the H1 hadronic energy scale, an alternative averaging is performed for which this uncertainty is considered as point-to-point uncorrelated. The difference between the alternative and nominal results is 0.9 % on average and reaches 8.7 % at low $x_{\mathbb{P}}$.

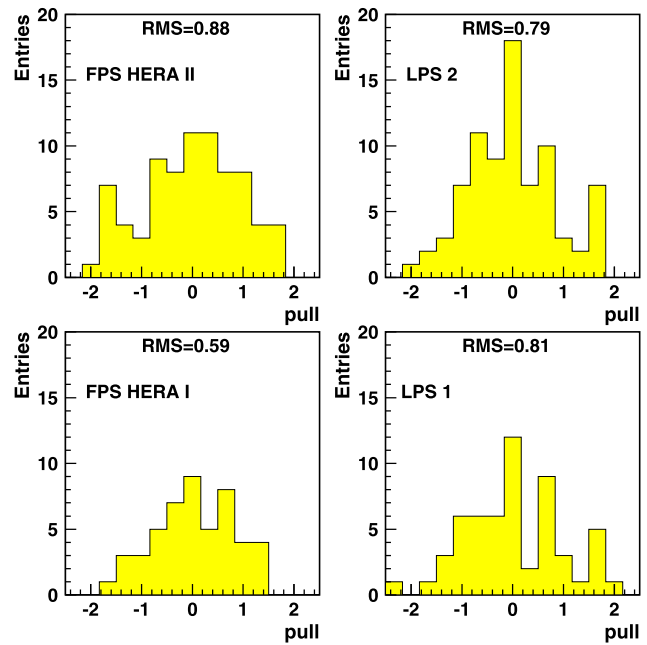


Fig. 3 Pull distributions for the individual data sets. The RMS values give the root mean square of the distributions

For each combined data point the difference between the average obtained by considering each of the procedural effects and the nominal average is calculated and summed in quadrature. The effect of the procedural uncertainties is 2.9 % on average and 9.3 % at most.

3 Results

In the minimisation procedure, 352 data points are combined to 191 cross section measurements. The data show good consistency, with $\chi^2_{\min}/n_{\text{dof}} = 133/161$. The distributions of pulls [10], shown in Fig. 3 for each data set, exhibit no significant tensions. For data with no correlated systematic uncertainties pulls are expected to follow Gaussian distributions with zero mean and unit width. Correlated systematic uncertainties lead to narrowed pull distributions.

The effects of the combination on the correlated systematic uncertainties are summarised in Table 3 in terms of shifts in units of the original uncertainty and of values of the final uncertainties as percentages of the originals. The combined cross section values are given in Table 4 together with statistical, uncorrelated systematic, correlated systematic, experimental, procedural and total uncertainties. The experimental uncertainty is obtained as the quadratic sum of the statistical, uncorrelated systematic and correlated systematic uncertainties. The total uncertainty is defined as the quadratic sum of the experimental and procedural uncertainties. The full information about correlations can be found

Table 4 Combined reduced cross sections $x_{\mathbb{P}}\sigma_r^{D(3)}(\beta, Q^2, x_{\mathbb{P}})$ for diffractive $ep \rightarrow eXp$. The values indicated by δ_{stat} , δ_{uncor} , δ_{cor} , δ_{exp} , δ_{proc} and δ_{tot} represent the statistical, uncorrelated systematic, correlated systematic, experimental, procedural and total uncertainties, respectively

Q^2 (GeV ²)	β	$x_{\mathbb{P}}$	$x_{\mathbb{P}}\sigma_r^{D(3)}$	δ_{stat} (%)	δ_{uncor} (%)	δ_{cor} (%)	δ_{exp} (%)	δ_{proc} (%)	δ_{tot} (%)
2.5	0.0018	0.0500	0.0110	19	5.8	4.7	21	7.6	22
2.5	0.0018	0.0750	0.0166	14	6.9	5.3	17	7.6	18
2.5	0.0018	0.0900	0.0128	14	9.6	5.1	18	7.9	20
2.5	0.0056	0.0085	0.0101	19	11	7.6	23	9.3	25
2.5	0.0056	0.0160	0.0093	12	6.9	5.1	14	3.9	15
2.5	0.0056	0.0250	0.0096	16	9.8	5.0	20	4.6	20
2.5	0.0056	0.0350	0.0110	18	11	4.9	22	2.3	22
2.5	0.0056	0.0500	0.0117	9.8	6.4	5.3	13	1.5	13
2.5	0.0056	0.0750	0.0143	14	11	5.7	19	4.7	19
2.5	0.0056	0.0900	0.0154	15	6.4	5.7	17	4.3	17
2.5	0.0178	0.0025	0.0099	14	6.8	4.5	16	8.2	18
2.5	0.0178	0.0085	0.0076	8.3	7.1	4.5	12	1.7	12
2.5	0.0178	0.0160	0.0073	8.2	9.5	4.5	13	1.4	13
2.5	0.0178	0.0250	0.0071	8.8	9.2	4.5	14	1.4	14
2.5	0.0178	0.0350	0.0095	15	29	4.9	33	2.3	33
2.5	0.0178	0.0500	0.0114	7.8	7.1	4.5	11	2.2	12
2.5	0.0178	0.0750	0.0123	11	7.8	4.9	14	1.7	14
2.5	0.0562	0.0009	0.0114	13	8.6	5.2	16	3.4	17
2.5	0.0562	0.0025	0.0074	9.3	5.7	4.8	12	2.8	12
2.5	0.0562	0.0085	0.0064	9.6	6.7	4.5	13	2.3	13
2.5	0.0562	0.0160	0.0068	10	10	4.6	15	4.4	16
2.5	0.0562	0.0250	0.0063	14	14	4.9	20	1.9	20
2.5	0.1780	0.0003	0.0156	8.8	5.4	4.7	11	2.6	12
2.5	0.1780	0.0009	0.0102	5.9	4.3	4.4	8.5	2.2	8.8
2.5	0.1780	0.0025	0.0068	8.0	6.3	4.7	11	2.6	12
2.5	0.1780	0.0085	0.0074	9.3	10	4.8	15	3.9	15
2.5	0.1780	0.0160	0.0116	18	7.5	5.0	20	2.3	20
2.5	0.5620	0.0003	0.0214	16	8.8	5.0	19	2.3	19
2.5	0.5620	0.0009	0.0172	19	23	5.0	31	2.3	31
2.5	0.5620	0.0025	0.0110	21	28	4.9	36	2.3	36
5.1	0.0018	0.0500	0.0199	5.9	0.0	6.6	8.9	1.8	9.1
5.1	0.0018	0.0750	0.0232	6.7	0.0	5.1	8.4	2.1	8.7
5.1	0.0056	0.0160	0.0135	3.9	0.6	5.9	7.1	2.0	7.4
5.1	0.0056	0.0250	0.0120	3.4	0.3	5.2	6.2	2.0	6.6
5.1	0.0056	0.0350	0.0134	4.0	0.6	4.7	6.2	1.5	6.3
5.1	0.0056	0.0500	0.0147	3.9	0.6	5.4	6.7	3.4	7.5
5.1	0.0056	0.0750	0.0180	5.7	1.3	6.1	8.4	3.7	9.2
5.1	0.0056	0.0900	0.0224	12	3.8	4.9	14	3.1	14
5.1	0.0178	0.0085	0.0120	2.6	0.4	5.9	6.4	7.6	10
5.1	0.0178	0.0160	0.0111	2.6	0.2	5.2	5.8	2.8	6.5
5.1	0.0178	0.0250	0.0109	3.0	0.5	5.2	6.0	2.2	6.4
5.1	0.0178	0.0350	0.0101	4.3	0.6	5.2	6.8	2.2	7.2
5.1	0.0178	0.0500	0.0134	4.1	1.4	5.1	6.7	2.2	7.0
5.1	0.0178	0.0750	0.0154	6.4	2.2	4.8	8.3	2.9	8.8
5.1	0.0562	0.0025	0.0107	2.4	0.2	5.0	5.6	3.4	6.8
5.1	0.0562	0.0085	0.0088	2.7	0.3	5.0	5.7	3.5	6.7
5.1	0.0562	0.0160	0.0088	3.2	0.3	5.1	6.0	2.7	6.6
5.1	0.0562	0.0250	0.0084	4.5	0.7	5.0	6.7	3.1	7.4

Table 4 (Continued)

Q^2 (GeV ²)	β	$x_{\mathbb{P}}$	$x_{\mathbb{P}}\sigma_r^{D(3)}$	δ_{stat} (%)	δ_{uncor} (%)	δ_{cor} (%)	δ_{exp} (%)	δ_{proc} (%)	δ_{tot} (%)
5.1	0.0562	0.0500	0.0095	16	13	4.9	21	1.9	21
5.1	0.0562	0.0750	0.0153	23	14	5.0	27	1.9	27
5.1	0.1780	0.0009	0.0121	11	7.4	4.9	14	11	18
5.1	0.1780	0.0025	0.0118	1.6	0.2	5.9	6.1	4.2	7.4
5.1	0.1780	0.0085	0.0095	2.8	0.5	5.0	5.8	3.5	6.7
5.1	0.1780	0.0160	0.0075	14	12	4.9	19	2.3	19
5.1	0.1780	0.0250	0.0107	13	13	4.9	20	1.9	20
5.1	0.1780	0.0350	0.0065	20	14	5.0	25	2.3	25
5.1	0.5620	0.0003	0.0275	13	8.2	4.9	16	2.3	16
5.1	0.5620	0.0009	0.0187	7.0	8.0	4.6	12	1.8	12
5.1	0.5620	0.0025	0.0153	1.4	0.1	6.1	6.2	6.1	8.7
5.1	0.5620	0.0085	0.0137	19	19	4.9	27	2.3	27
8.8	0.0018	0.0750	0.0288	12	0.0	6.2	13	1.5	13
8.8	0.0056	0.0250	0.0152	5.0	0.8	5.1	7.2	2.0	7.5
8.8	0.0056	0.0350	0.0171	5.1	1.2	4.9	7.2	1.7	7.4
8.8	0.0056	0.0500	0.0197	4.1	1.2	4.6	6.3	1.6	6.5
8.8	0.0056	0.0750	0.0212	5.9	1.1	4.8	7.7	3.8	8.6
8.8	0.0056	0.0900	0.0281	9.6	4.4	5.0	12	5.7	13
8.8	0.0178	0.0085	0.0128	4.2	0.9	5.1	6.7	4.0	7.8
8.8	0.0178	0.0160	0.0124	3.1	0.6	4.9	5.8	1.5	6.0
8.8	0.0178	0.0250	0.0133	3.4	0.6	4.8	5.9	1.5	6.1
8.8	0.0178	0.0350	0.0130	4.5	0.5	4.8	6.6	1.4	6.8
8.8	0.0178	0.0500	0.0159	3.8	1.0	4.6	6.1	1.5	6.3
8.8	0.0178	0.0750	0.0162	5.6	1.7	4.8	7.6	2.3	8.0
8.8	0.0178	0.0900	0.0220	9.5	5.9	5.0	12	2.7	13
8.8	0.0562	0.0025	0.0125	3.4	0.4	5.0	6.1	3.8	7.1
8.8	0.0562	0.0085	0.0106	3.2	0.6	5.0	6.0	2.0	6.3
8.8	0.0562	0.0160	0.0108	2.9	0.2	5.0	5.8	2.7	6.4
8.8	0.0562	0.0250	0.0098	3.6	0.5	5.0	6.2	2.5	6.7
8.8	0.0562	0.0350	0.0109	5.2	0.0	4.9	7.2	2.1	7.5
8.8	0.0562	0.0500	0.0144	5.1	1.1	5.1	7.3	2.4	7.7
8.8	0.0562	0.0750	0.0140	11	4.3	4.6	12	1.7	13
8.8	0.1780	0.0009	0.0177	7.7	2.7	5.0	9.6	1.6	9.7
8.8	0.1780	0.0025	0.0129	2.3	0.4	5.1	5.6	2.5	6.1
8.8	0.1780	0.0085	0.0104	2.6	0.4	4.6	5.3	2.7	5.9
8.8	0.1780	0.0160	0.0090	3.9	0.7	5.3	6.6	2.6	7.1
8.8	0.1780	0.0250	0.0098	14	14	4.9	21	1.9	21
8.8	0.1780	0.0350	0.0103	17	11	4.9	21	2.3	21
8.8	0.1780	0.0500	0.0116	12	8.3	4.5	15	1.8	16
8.8	0.5620	0.0003	0.0250	7.1	4.2	4.4	9.3	8.9	13
8.8	0.5620	0.0009	0.0207	5.6	3.5	4.4	7.9	6.7	10
8.8	0.5620	0.0025	0.0166	1.6	0.1	6.1	6.3	8.3	10
8.8	0.5620	0.0085	0.0142	8.5	4.3	4.3	10	8.0	13
8.8	0.5620	0.0160	0.0102	17	13	4.4	22	2.3	22
15.3	0.0056	0.0500	0.0245	6.7	2.2	4.9	8.6	1.1	8.7
15.3	0.0056	0.0750	0.0296	10	0.0	5.7	12	1.6	12
15.3	0.0178	0.0160	0.0176	4.8	0.7	5.0	7.0	2.4	7.4
15.3	0.0178	0.0250	0.0164	4.4	0.7	4.8	6.6	2.4	7.0

Table 4 (Continued)

Q^2 (GeV ²)	β	$x_{\mathbb{P}}$	$x_{\mathbb{P}}\sigma_r^{D(3)}$	δ_{stat} (%)	δ_{uncor} (%)	δ_{cor} (%)	δ_{exp} (%)	δ_{proc} (%)	δ_{tot} (%)
15.3	0.0178	0.0350	0.0165	5.7	1.1	4.7	7.5	1.4	7.6
15.3	0.0178	0.0500	0.0176	4.9	1.4	4.8	7.0	2.2	7.4
15.3	0.0178	0.0750	0.0211	6.7	2.1	4.8	8.5	2.6	8.9
15.3	0.0178	0.0900	0.0234	10	1.6	4.8	11	3.3	12
15.3	0.0562	0.0085	0.0134	4.5	0.0	6.0	7.5	6.1	9.7
15.3	0.0562	0.0160	0.0122	3.9	0.3	4.9	6.3	2.5	6.8
15.3	0.0562	0.0250	0.0113	4.5	0.3	4.8	6.6	1.0	6.7
15.3	0.0562	0.0350	0.0121	6.2	0.0	5.0	8.0	2.0	8.2
15.3	0.0562	0.0500	0.0140	5.7	1.1	4.9	7.6	2.0	7.8
15.3	0.0562	0.0750	0.0174	7.6	1.4	4.7	9.1	2.1	9.3
15.3	0.0562	0.0900	0.0162	10	3.6	5.1	12	2.8	12
15.3	0.1780	0.0025	0.0136	3.4	0.5	5.0	6.0	1.3	6.2
15.3	0.1780	0.0085	0.0111	3.4	0.5	4.8	5.9	2.2	6.2
15.3	0.1780	0.0160	0.0098	3.9	0.6	5.0	6.4	2.2	6.8
15.3	0.1780	0.0250	0.0097	6.1	0.9	5.2	8.1	2.4	8.4
15.3	0.1780	0.0350	0.0117	15	17	4.9	23	2.3	23
15.3	0.1780	0.0500	0.0134	12	15	4.9	20	2.3	20
15.3	0.5620	0.0009	0.0180	8.8	3.4	4.6	11	3.3	11
15.3	0.5620	0.0025	0.0173	2.5	0.2	5.8	6.3	3.5	7.2
15.3	0.5620	0.0085	0.0162	3.3	0.5	5.1	6.1	3.0	6.8
15.3	0.5620	0.0160	0.0151	17	14	4.9	22	2.3	22
15.3	0.5620	0.0350	0.0094	20	21	4.9	30	2.3	30
26.5	0.0056	0.0750	0.0359	17	0.0	5.3	18	3.2	18
26.5	0.0178	0.0250	0.0179	8.0	1.4	4.8	9.4	2.3	9.7
26.5	0.0178	0.0350	0.0202	8.6	0.0	5.3	10	1.6	10
26.5	0.0178	0.0500	0.0250	6.7	1.3	4.8	8.4	1.8	8.6
26.5	0.0178	0.0750	0.0249	10	2.3	5.2	12	2.6	12
26.5	0.0562	0.0085	0.0157	6.6	1.2	5.3	8.6	8.0	12
26.5	0.0562	0.0160	0.0150	4.9	0.7	4.8	7.0	1.8	7.2
26.5	0.0562	0.0250	0.0134	5.5	0.7	4.5	7.1	1.3	7.3
26.5	0.0562	0.0350	0.0157	7.4	0.0	4.8	8.8	1.6	9.0
26.5	0.0562	0.0500	0.0184	6.2	1.6	5.1	8.2	1.3	8.3
26.5	0.0562	0.0750	0.0211	7.4	1.8	4.5	8.9	1.5	9.0
26.5	0.0562	0.0900	0.0237	9.6	3.2	5.0	11	3.4	12
26.5	0.1780	0.0025	0.0138	5.4	0.4	5.1	7.5	1.4	7.6
26.5	0.1780	0.0085	0.0126	5.0	0.8	4.8	7.0	2.7	7.5
26.5	0.1780	0.0160	0.0113	5.5	0.0	5.1	7.6	2.2	7.9
26.5	0.1780	0.0250	0.0093	6.5	1.0	4.9	8.2	1.4	8.3
26.5	0.1780	0.0350	0.0100	9.8	0.0	5.7	11	4.0	12
26.5	0.1780	0.0500	0.0105	26	14	4.9	30	1.9	30
26.5	0.1780	0.0750	0.0169	42	11	4.9	44	1.9	44
26.5	0.5620	0.0009	0.0241	22	10	4.9	25	1.9	25
26.5	0.5620	0.0025	0.0189	3.7	0.2	6.0	7.0	9.1	12
26.5	0.5620	0.0085	0.0140	4.3	0.4	5.0	6.6	3.8	7.6
26.5	0.5620	0.0250	0.0136	31	15	4.9	35	1.9	35
46	0.0178	0.0500	0.0313	8.6	4.5	4.7	11	1.6	11
46	0.0178	0.0750	0.0218	19	0.0	5.1	20	2.5	20
46	0.0562	0.0160	0.0163	8.8	0.0	5.2	10	2.1	11

Table 4 (Continued)

Q^2 (GeV ²)	β	$x_{\mathbb{P}}$	$x_{\mathbb{P}}\sigma_r^{D(3)}$	δ_{stat} (%)	δ_{uncor} (%)	δ_{cor} (%)	δ_{exp} (%)	δ_{proc} (%)	δ_{tot} (%)
46	0.0562	0.0250	0.0172	8.6	0.0	5.3	10	2.1	10
46	0.0562	0.0350	0.0158	8.3	1.8	4.6	9.6	2.2	9.8
46	0.0562	0.0500	0.0199	7.6	1.9	4.8	9.2	2.8	9.6
46	0.0562	0.0750	0.0212	8.4	1.2	4.9	9.7	3.2	10
46	0.0562	0.0900	0.0267	8.9	2.4	4.8	10	1.0	10
46	0.1780	0.0085	0.0121	6.6	1.3	5.4	8.6	2.1	8.9
46	0.1780	0.0160	0.0133	5.9	1.5	4.8	7.7	2.4	8.1
46	0.1780	0.0250	0.0135	8.5	0.0	4.9	9.8	2.2	10
46	0.1780	0.0350	0.0129	7.5	1.9	4.6	9.0	2.1	9.2
46	0.1780	0.0500	0.0148	7.4	2.9	4.8	9.3	2.4	9.6
46	0.1780	0.0750	0.0201	9.9	4.0	4.7	12	3.4	12
46	0.1780	0.0900	0.0177	13	4.2	5.0	14	8.6	17
46	0.5620	0.0025	0.0196	5.1	1.0	5.4	7.5	4.2	8.6
46	0.5620	0.0085	0.0135	5.1	1.0	4.9	7.2	4.6	8.5
46	0.5620	0.0160	0.0124	6.9	1.8	4.8	8.6	2.3	8.9
46	0.5620	0.0250	0.0106	13	0.0	5.9	14	1.2	15
46	0.5620	0.0350	0.0135	14	7.0	4.8	16	2.2	16
46	0.5620	0.0500	0.0120	17	20	4.9	26	2.3	26
46	0.8160	0.0009	0.0145	21	5.3	4.5	22	1.4	22
46	0.8160	0.0025	0.0131	17	8.1	5.3	20	3.0	20
46	0.8160	0.0085	0.0110	18	3.9	4.3	19	1.5	19
46	0.8160	0.0160	0.0092	27	3.9	5.4	28	4.1	28
80	0.0562	0.0350	0.0227	19	0.0	5.8	20	2.7	20
80	0.0562	0.0500	0.0235	15	0.0	5.0	16	2.0	16
80	0.0562	0.0750	0.0216	24	0.0	5.9	25	1.9	25
80	0.1780	0.0085	0.0206	15	0.0	6.0	16	2.9	16
80	0.1780	0.0160	0.0133	13	0.0	4.8	14	2.3	14
80	0.1780	0.0250	0.0146	12	0.0	5.2	13	1.6	13
80	0.1780	0.0350	0.0162	14	0.0	5.6	15	1.0	15
80	0.1780	0.0500	0.0146	15	0.0	5.5	16	2.3	16
80	0.1780	0.0750	0.0183	26	0.0	5.3	27	3.0	27
80	0.5620	0.0085	0.0116	10	0.0	6.4	12	5.1	13
80	0.5620	0.0160	0.0090	14	0.0	7.0	15	3.5	16
80	0.5620	0.0250	0.0104	17	0.0	6.7	18	5.3	19
80	0.5620	0.0350	0.0109	25	0.0	7.3	26	3.6	26
200	0.0562	0.0500	0.0162	28	0.0	5.0	28	1.0	28
200	0.0562	0.0750	0.0288	37	0.0	5.5	37	2.3	37
200	0.1780	0.0160	0.0145	20	0.0	5.8	21	1.3	21
200	0.1780	0.0250	0.0199	16	0.0	5.0	17	1.9	17
200	0.1780	0.0350	0.0169	22	0.0	5.2	23	2.6	23
200	0.1780	0.0500	0.0235	20	0.0	5.5	21	2.6	21
200	0.1780	0.0750	0.0209	35	0.0	5.6	35	2.5	36
200	0.5620	0.0085	0.0109	19	0.0	6.6	21	3.9	21
200	0.5620	0.0160	0.0093	23	0.0	6.4	24	1.9	24
200	0.5620	0.0250	0.0074	27	0.0	6.7	28	4.9	29
200	0.5620	0.0350	0.0158	33	0.0	6.7	34	2.4	34
200	0.5620	0.0500	0.0151	29	0.0	5.4	29	1.8	29
200	0.5620	0.0750	0.0228	50	0.0	5.9	50	3.2	50

elsewhere.³ As the global normalisations of the input data sets are fitted as correlated systematic uncertainties, the normalisation uncertainty on the combined data is included in the correlated systematic uncertainty given in Table 4.

Most of the 23 correlated systematic uncertainties shift by less than 0.5σ of the nominal value in the averaging procedure. None of them shifts by substantially more than 1σ , with the exception of the hadronic energy scale for $x_{\mathbb{P}} < 0.012$ for the ‘FPS HERA II’ sample. Detailed studies show that there is a tension between the H1 ‘FPS HERA II’ and ZEUS ‘LPS 2’ data at low $x_{\mathbb{P}}$; the average ratio of the H1 to ZEUS cross sections is above 1.0 for $\beta > 0.1$ and below 0.9 for $\beta < 0.1$. The H1 cross section uncertainty is positively correlated with the hadronic energy scale for $\beta > 0.1$ and anti-correlated for $\beta < 0.1$. As a result, the combination shifts the H1 cross sections for $x_{\mathbb{P}} < 0.012$ in the direction opposite to the cross section uncertainty due to the H1 hadronic energy scale. Conversely the combined statistical and uncorrelated uncertainty on the ZEUS data is much larger than the ZEUS hadronic energy scale uncertainty; consequently the fit is less sensitive to the ZEUS hadronic energy scale.

The influence of several correlated systematic uncertainties is reduced significantly for the combined result. Specifically, the uncertainty on the FPS proton energy measurement and the normalisation uncertainties on the ‘FPS HERA I’ and ‘LPS 1’ samples are reduced by more than a factor of 2. The H1 hadronic energy scale uncertainty for the low $x_{\mathbb{P}}$ -range ($x_{\mathbb{P}} < 0.012$) and the ZEUS hadronic energy scale uncertainty are reduced to around 55 % of those for the individual data sets. Since H1 and ZEUS use different reconstruction methods, similar systematic sources influence the measured cross section differently. Therefore, requiring the cross sections to be consistent at all $(\beta, Q^2, x_{\mathbb{P}})$ points constrains the systematic uncertainties efficiently. Due to this cross calibration effect, the combined measurement shows an average improvement of the experimental uncertainty of about 27 % with respect to the most precise single data set, ‘FPS HERA II’, though the latter data set contains five times more events than the second largest data set, ‘LPS 2’. The correlated part of the experimental uncertainty is reduced from about 69 % in [2] to 49 % in the combined measurement. The statistical, experimental and procedural uncertainties on the combined data are on average 11 %, 13.8 % and 2.9 %, respectively. The total uncertainty on the cross section is 14.3 % on average and is 6 % for the most precise points. The normalisation uncertainty, which contributes to the correlated systematic uncertainty on the combined data, is on average 4 %. The combined result extends the kinematic coverage with respect to the H1 and ZEUS measurements taken separately and the resulting cross section covers

³The combined data together with the full correlation information are provided at the URL. <http://www.desy.de/h1zeus>

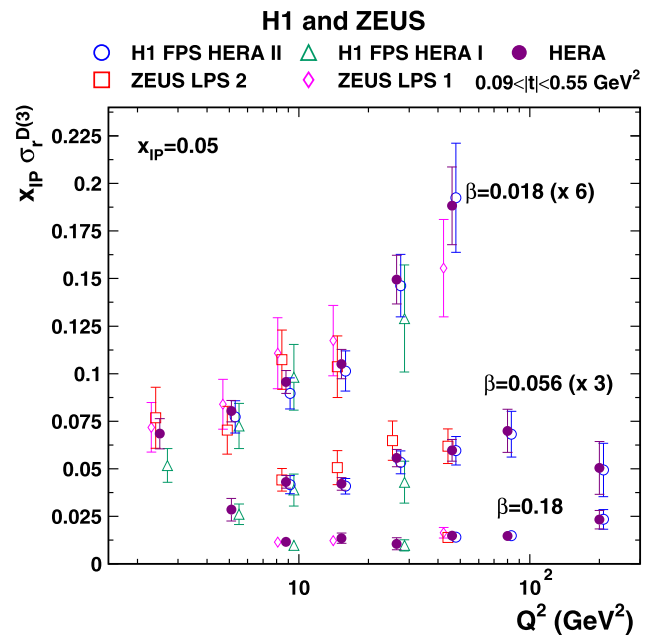


Fig. 4 Reduced diffractive cross section $x_{\mathbb{P}} \sigma_r^{D(3)}(\beta, Q^2, x_{\mathbb{P}})$ for $0.09 < |t| < 0.55 \text{ GeV}^2$ as a function of Q^2 for different values of β at $x_{\mathbb{P}} = 0.05$. The HERA combined data are compared to the H1 and ZEUS data inputs to the averaging procedure. The *error bars* indicate the statistical and systematic uncertainties added in quadrature for the input measurements and the statistical, systematic and procedural uncertainties added in quadrature for the combined points. Normalisation uncertainties are not included in the error bars of the individual measurements, whereas they are included in the *error bars* of the combined points

the region $2.5 \leq Q^2 \leq 200 \text{ GeV}^2$, $0.0018 \leq \beta \leq 0.816$ and $0.00035 \leq x_{\mathbb{P}} \leq 0.09$, for $0.09 < |t| < 0.55 \text{ GeV}^2$. Figure 4 shows the HERA combined cross section as a function of Q^2 at $x_{\mathbb{P}} = 0.05$, for different values of β , compared with the individual measurements used for the combination. The reduction of the total uncertainty of the HERA measurement compared to the input cross sections is visible. The derivative of the reduced cross section as a function of $\log(Q^2)$ decreases with β , a feature characteristic of the scaling violations in diffractive DIS, which are now measured precisely from proton-tagged as well as LRG data. Figures 5 and 6 show the HERA combined diffractive reduced cross sections as a function of Q^2 and $x_{\mathbb{P}}$, respectively.

At low $x_{\mathbb{P}} \lesssim 0.01$, where the proton spectrometer data are free from proton dissociation contributions, the combined data provide the most precise determination of the absolute normalisation of the diffractive cross section.

4 Conclusions

The reduced diffractive cross sections, $\sigma_r^{D(3)}(ep \rightarrow eXp)$, measured by the H1 and ZEUS Collaborations by using proton spectrometers to detect the leading protons are com-

Fig. 5 HERA combined reduced diffractive cross section $x_{\mathbb{P}} \sigma_r^{D(3)}(\beta, Q^2, x_{\mathbb{P}})$ for $0.09 < |t| < 0.55 \text{ GeV}^2$ as a function of Q^2 for different values of β and $x_{\mathbb{P}}$. The error bars indicate the statistical, systematic and procedural uncertainties added in quadrature. The normalisation uncertainty is included

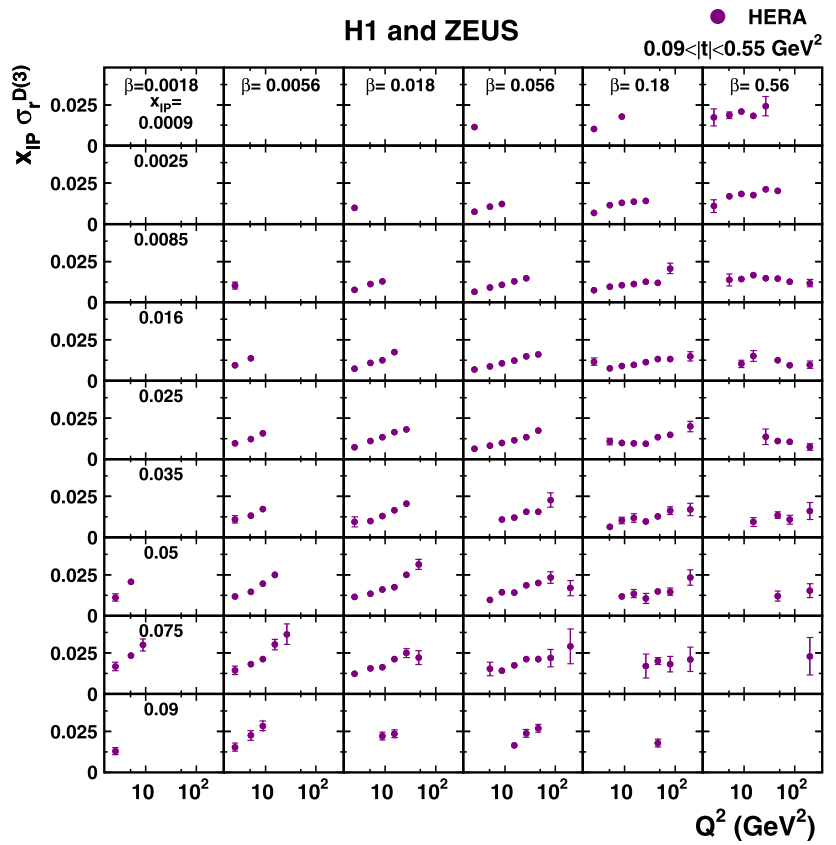
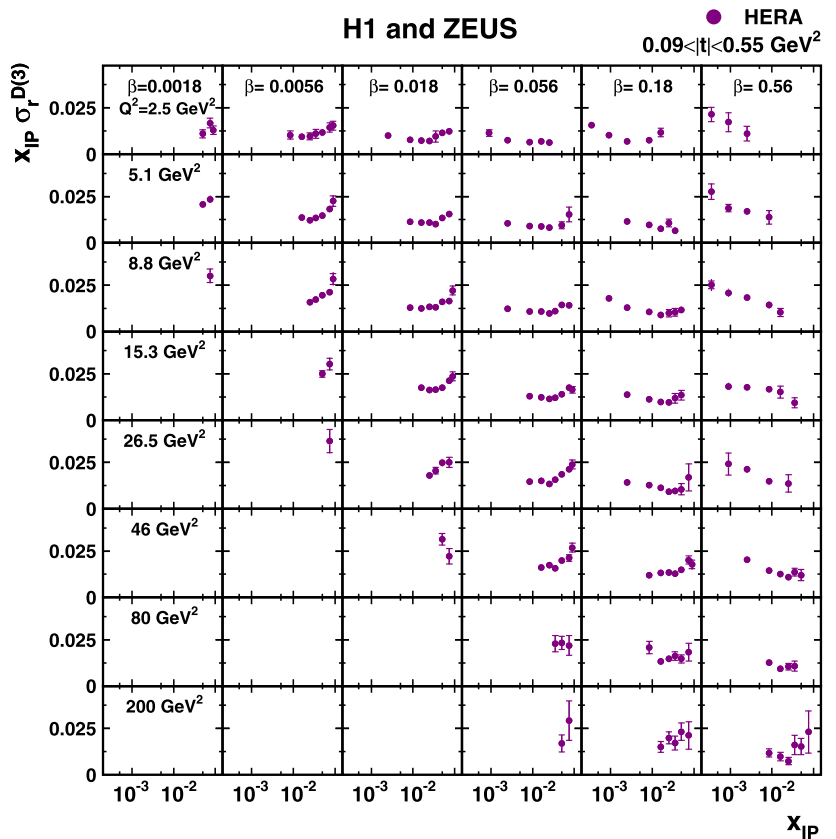


Fig. 6 HERA combined reduced diffractive cross section $x_{\mathbb{P}} \sigma_r^{D(3)}(\beta, Q^2, x_{\mathbb{P}})$ for $0.09 < |t| < 0.55 \text{ GeV}^2$ as a function of $x_{\mathbb{P}}$ for different values of β and Q^2 . The error bars indicate the statistical, systematic and procedural uncertainties added in quadrature. The normalisation uncertainty is included



bined. The input data from the two experiments are consistent with a $\chi_{\min}^2/n_{\text{dof}} = 133/161$. The combination of the measurements results in more precise and kinematically extended diffractive DIS data in the t -range $0.09 < |t| < 0.55 \text{ GeV}^2$. The total uncertainty on the cross section measurement is 6 % for the most precise points. The combined data provide the most precise determination of the absolute normalisation of the $ep \rightarrow eXp$ cross section.

Acknowledgements We are grateful to the HERA machine group whose outstanding efforts have made these experiments possible. We appreciate the contributions to the construction and maintenance of the H1 and ZEUS detectors of many people who are not listed as authors. We thank our funding agencies for financial support, the DESY technical staff for continuous assistance and the DESY directorate for their support and for the hospitality they extended to the non-DESY members of the collaborations.

Open Access This article is distributed under the terms of the Creative Commons Attribution License which permits any use, distribution, and reproduction in any medium, provided the original author(s) and the source are credited.

References

1. A. Aktas et al. (H1 Collaboration), *Eur. Phys. J. C* **48**, 749 (2006)
2. A. Aktas et al. (H1 Collaboration), *Eur. Phys. J. C* **71**, 1578 (2011)
3. S. Chekanov et al. (ZEUS Collaboration), *Eur. Phys. J. C* **38**, 43 (2004)
4. S. Chekanov et al. (ZEUS Collaboration), *Nucl. Phys. B* **816**, 1 (2009)
5. A. Aktas et al. (H1 Collaboration), *Eur. Phys. J. C* **48**, 715 (2006)
6. F.D. Aaron et al. (H1 Collaboration), *Eur. Phys. J. C* **72**, 2074 (2012)
7. P. Newman, M. Ruspa, [arXiv:0903.2957](https://arxiv.org/abs/0903.2957)
8. A. Glazov, *AIP Conf. Proc.* **792**, 237 (2005)
9. F.D. Aaron et al. (H1 Collaboration), *Eur. Phys. J. C* **63**, 625 (2009)
10. F.D. Aaron et al. (H1 and ZEUS Collaborations), *J. High Energy Phys.* **1001**, 109 (2010)
11. I. Abt et al. (H1 Collaboration), *Nucl. Instrum. Methods Phys. Res. A* **386**, 310 (1997)
12. I. Abt et al. (H1 Collaboration), *Nucl. Instrum. Methods Phys. Res. A* **386**, 348 (1997)
13. R.D. Appuhn et al. (H1 SPACAL Group), *Nucl. Instrum. Methods Phys. Res. A* **386**, 397 (1997)
14. U. Holm (ed.) (ZEUS Collaboration), *The ZEUS detector*. Status Report (unpublished), DESY, 1993. Available on <http://www-zeus.desy.de/bluebook/bluebook.html>
15. S. Chekanov et al. (ZEUS Collaboration), *Nucl. Phys. B* **831**, 1 (2010)